Theory of magnetoresistance of organic molecular tunnel junctions with nonmagnetic electrodes

Sha Shi,[1,*] Zuoti Xie,[2] Feilong Liu,[1,†] Darryl L. Smith,[1] C. Daniel Frisbie,[2] and P. Paul Ruden[1]
[1]*Department of Electrical and Computer Engineering, University of Minnesota, Minneapolis, Minnesota 55455, USA*
[2]*Department of Chemical Engineering and Materials Science, University of Minnesota, Minneapolis, Minnesota 55455, USA*
(Received 2 February 2017; published 26 April 2017)

Large room-temperature magnetoresistance observed for devices composed of self-assembled monolayers of different oligophenylene thiols sandwiched between gold contacts has recently been reported [Z. Xie, S. Shi, F. Liu, D. L. Smith, P. P. Ruden, and C. D. Frisbie, ACS Nano **10**, 8571 (2016)]. The transport mechanism through the organic molecules was determined to be nonresonant tunneling. To explain this kind of magnetoresistance, we develop an analytical model based on the interaction of the tunneling charge carrier with an unpaired charge carrier populating a contact-molecule interface state. The Coulomb interaction between carriers causes the transmission coefficients to depend on their relative spin orientation. Singlet and triplet pairing of the tunneling and the interface carriers thus correspond to separate conduction channels with different transmission probabilities. Spin relaxation enabling transitions between the different channels, and therefore tending to maximize the tunneling current for a given applied bias, can be suppressed by relatively small magnetic fields, leading to large magnetoresistance. Our model elucidates how the Coulomb interaction gives rise to transmission probabilities that depend on spin and how an applied magnetic field can inhibit transitions between different spin configurations.

DOI: 10.1103/PhysRevB.95.155315

I. INTRODUCTION

Certain molecules, such as oligophenylene thiols, bond in oriented fashion to gold substrates and lend themselves to the formation of well-defined self-assembled monolayers (SAMs) [1]. Charge transport through the molecules can be explored experimentally by contacting the metal substrate, making a soft electrical contact to the exposed side of the SAM, and applying bias [2,3]. The conductance of these SAM-based molecular junctions is a topic of intense investigation and different transport mechanisms such as tunneling and hopping have been observed [4,5]. While SAM-based experiments of molecular charge transport measure the parallel conductance of roughly 100 molecules, other techniques have focused on single molecules [6,7].

The metal-molecule-metal junction electrical measurements have also addressed magnetic field effects. In particular, the Kondo effect has been observed in low-temperature (typically 10 K) experiments on single molecules under relatively large applied magnetic fields (typically several Tesla) [8,9]. The effect is a consequence of spin correlation between the charge carriers in the contact and in the molecule. This interaction leads to a conductance characterized by a zero-bias resonance, which is sensitive to an applied magnetic field.

On the other hand, recent experiments on relatively short oligophenylene thiol molecule SAMs have led to the observation of significant zero-bias, room-temperature magnetoresistance (MR) at low applied magnetic fields (0.1 T) [10]. The transport was shown to be due to nonresonant tunneling by comparing the conductances of molecules of different lengths, and the relative MR was found to be essentially independent of the length of the molecule and also independent of the direction of the magnetic field. Conventional, single-particle effects do not explain these observed phenomena for the following reasons.

(1) The electron energy scale associated with a magnetic field is on the order of 0.1 meV/T, i.e., negligible compared to the tunneling barrier and the thermal energy for the small magnetic field applied.

(2) The length scale of the confinement potential associated with the weak magnetic field is large compared to the size of the molecules.

(3) Any modulation of the overlap of wave functions involved in the tunneling process should dependent on the direction of the magnetic field.

The experimental observations are therefore attributed to an effect not considered in an independent particle treatment, here specifically the interaction between a tunneling charge carrier and an unpaired charge carrier in the molecule. Density functional calculations and experiments have provided ample evidence that the chemisorption of aromatic thiols on metals can lead to charge transfer, i.e., localized charge on the molecule and compensating charge in the metal [11–13]. It is the aim of this paper to present a more complete analytical model for the experimental MR results reported, and to explore different parameter sets that may be relevant for different molecules. In Sec. II the models for the tunneling transmission coefficients and subsequently for the carrier distribution over the different transmission channels are developed. Section III presents example results, and Sec. IV summarizes the conclusions. The presentation here is in terms of electron tunneling. However, the model developed has electron-hole symmetry and in a simplified version was used to explain hole-tunneling MR phenomena in Ref. [10].

II. THEORY

A. The tunneling process

The analytical model for molecular tunneling to be developed in this paper describes a molecule in contact with

*Corresponding author: shixx262@umn.edu
†Present address: Eindhoven University of Technology, 5600 MB Eindhoven, The Netherlands.

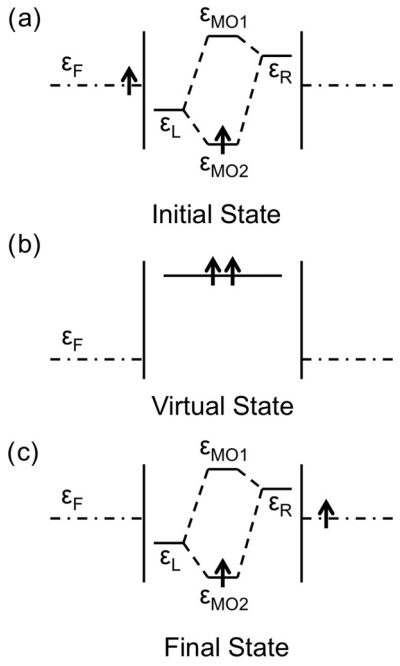

FIG. 1. Schematic representation of an electron tunneling through the organic molecule. For the case shown the spins of the tunneling electron and the unpaired "interface state" electron are parallel. (a–c) Energy-level diagrams for the initial, intermediate (virtual), and final states, respectively.

metal contacts at both ends. The model molecule has two distinct single-electron energy levels. Both levels are twofold spin degenerate, and the lower level is occupied by one electron of either spin orientation. We refer to this state as the "interface state" and associate its formation and occupation by an unpaired electron with the charge transfer that occurs when the molecule bonds with one of the metal contacts, e.g., via a thiol-Au bond that enables the SAM to form. The interface state energy level therefore lies below the metal contact Fermi energy [12]. Tunneling through the molecule is enabled by a virtual two-electron state, the energy level of which lies above the metal Fermi energy due to the mutual Coulomb interaction of the two electrons. This energy level depends on the total spin of the two electrons. As a consequence, the tunneling barrier seen by an electron depends on its spin. A schematic energy-level diagram for the electron transfer between the two metal contacts is shown in Fig. 1. Under bias, an electron arrives at the nonmagnetic emitter-molecule interface with randomly oriented spin ($|\uparrow\rangle$ or $|\downarrow\rangle$). Together with the unpaired localized electron in the interface state it forms singlet and triplet states, defined as $|S\rangle = (|\uparrow\downarrow\rangle - |\downarrow\uparrow\rangle)/\sqrt{2}$, $|T_0\rangle = (|\uparrow\downarrow\rangle + |\downarrow\uparrow\rangle)/\sqrt{2}$, $|T_+\rangle = |\uparrow\uparrow\rangle$, $|T_-\rangle = |\downarrow\downarrow\rangle$, where the second spin orientation symbol always refers to the electron in the interface state. (The specific example depicted in Fig. 1 shows

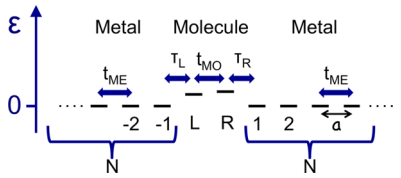

FIG. 2. Linear chain model for the molecule (sites L and R) and the metal emitter ($n < 0$) and collector ($n > 0$) contacts. Also indicated are the energy levels associated with the local orbitals and the different intersite transfer-matrix elements.

the tunneling of an electron based on the virtual intermediate state $|\uparrow\uparrow\rangle$.) We assume that the spin is conserved during the tunneling process. Hence, nonresonant tunneling is enabled by the virtual occupation of the corresponding two-electron molecular state, i.e., either singlet or triplet.

The system composed of the metal contacts and the molecule is modeled with the aid of a one-dimensional chain of interacting localized states [14], as is shown in Fig. 2. The molecule is represented by two sites, L and R, and the left and right metal contacts are represented by sites $n < 0$ and $n > 0$, respectively.

We assume that the parameters are such that nonresonant tunneling at the contact metal Fermi energy adequately describes the transport process. First we explore the single-electron and two-electron states of the isolated molecule. The former are simply found by diagonalizing the Hamiltonian:

$$H_{\mathrm{MO}} = \varepsilon_L c_L^+ c_L + \varepsilon_R c_R^+ c_R - t_{\mathrm{MO}}(c_L^+ c_R + \mathrm{H.c.}) \qquad (1)$$

where $\varepsilon_{L,R}$ represent the energy levels associated with two sites,$-t_{\mathrm{MO}} = \langle\psi_L|H_{\mathrm{MO}}|\psi_R\rangle$ is the transfer-matrix element between the two sites, and ψ_L and ψ_R represent the spatial wave functions. Diagonalization yields

$$\varepsilon_{\mathrm{MO},+,-} = \frac{\varepsilon_L + \varepsilon_R \pm \sqrt{\Delta^2 + 4t_{\mathrm{MO}}^2}}{2}. \qquad (2)$$

Here, $\Delta = \varepsilon_R - \varepsilon_L$. As indicated above, we refer to the lower level as the interface state, which is occupied by an unpaired electron in equilibrium. $|\psi_{M-}\rangle$ represents that single-electron state in the molecule:

$$|\psi_{M-}\rangle = a_{L-}|\psi_L\rangle + a_{R-}|\psi_R\rangle. \qquad (3)$$

Next, we calculate the molecular two-electron states. Since the two electrons are in close proximity, their Coulomb interaction is strong and can lead to a large singlet/triplet splitting. To explore this, we consider the spin explicitly and include the interaction $e^2/|\vec{r^1} - \vec{r^2}|$ between electrons 1 and 2, labeled by superscripts. There are four single-electron states: $|\psi_L\rangle|\uparrow\rangle$, $|\psi_L\rangle|\downarrow\rangle$, $|\psi_R\rangle|\uparrow\rangle$, and $|\psi_R\rangle|\downarrow\rangle$, hence six two-electron states can be formed:

Singlet states:

$$\left.\begin{aligned} |S_{LL}\rangle &= |\psi_L^1\rangle|\psi_L^2\rangle \\ |S_{RR}\rangle &= |\psi_R^1\rangle|\psi_R^2\rangle \\ |S_{LR}\rangle &= \tfrac{1}{\sqrt{2}}\left(|\psi_L^1\rangle|\psi_R^2\rangle + |\psi_R^1\rangle|\psi_L^2\rangle\right) \end{aligned}\right\} \frac{1}{\sqrt{2}}(|\uparrow^1\rangle|\downarrow^2\rangle - |\downarrow^1\rangle|\uparrow^2\rangle). \qquad (4a)$$

Triplet states:

$$\left.\begin{matrix}|T_+\rangle \\ |T_-\rangle \\ |T_0\rangle\end{matrix}\right\} = \frac{1}{\sqrt{2}}\left(|\psi_L^1\rangle|\psi_R^2\rangle - |\psi_R^1\rangle|\psi_L^2\rangle\right)\begin{cases}|\uparrow^1\rangle|\uparrow^2\rangle \\ |\downarrow^1\rangle|\downarrow^2\rangle \\ \frac{1}{\sqrt{2}}(|\uparrow^1\rangle|\downarrow^2\rangle + |\downarrow^1\rangle|\uparrow^2\rangle)\end{cases}. \tag{4b}$$

The Hamiltonian is not spin dependent. Thus, the 6×6 Hamiltonian matrix with singlet and triplet basis states block diagonalizes into two 3×3 blocks as follows:

$$\begin{array}{c} \text{Singlet matrix:} \\ \langle S_{LL}| \\ \langle S_{RR}| \\ \langle S_{LR}| \end{array} \begin{array}{c} |S_{LL}\rangle \\ \\ \\ \end{array} \begin{array}{c} |S_{RR}\rangle \\ \\ \\ \end{array} \begin{array}{c} |S_{LR}\rangle \\ \\ \\ \end{array} \begin{bmatrix} 2\varepsilon_L + U & J & \sqrt{2}(-t_{\mathrm{MO}} + D) \\ J & 2\varepsilon_R + U & \sqrt{2}(-t_{\mathrm{MO}} + D) \\ \sqrt{2}(-t_{\mathrm{MO}} + D) & \sqrt{2}(-t_{\mathrm{MO}} + D) & \varepsilon_L + \varepsilon_R + C + J \end{bmatrix}. \tag{5a}$$

$$\begin{array}{c} \text{Triplet matrix:} \\ \langle T_0| \\ \langle T_+| \\ \langle T_-| \end{array} \begin{array}{c} |T_0\rangle \\ \\ \\ \end{array} \begin{array}{c} |T_+\rangle \\ \\ \\ \end{array} \begin{array}{c} |T_-\rangle \\ \\ \\ \end{array} \begin{bmatrix} \varepsilon_L + \varepsilon_R + C - J & 0 & 0 \\ 0 & \varepsilon_L + \varepsilon_R + C - J & 0 \\ 0 & 0 & \varepsilon_L + \varepsilon_R + C - J \end{bmatrix}. \tag{5b}$$

Here,

$$U = \langle \psi_L^1 \psi_L^2 | \frac{e^2}{|\vec{r^1} - \vec{r^2}|} | \psi_L^1 \psi_L^2 \rangle = \langle \psi_R^1 \psi_R^2 | \frac{e^2}{|\vec{r^1} - \vec{r^2}|} | \psi_R^1 \psi_R^2 \rangle, \tag{6a}$$

$$C = \langle \psi_L^1 \psi_R^2 | \frac{e^2}{|\vec{r^1} - \vec{r^2}|} | \psi_L^1 \psi_R^2 \rangle, \tag{6b}$$

$$D = \langle \psi_L^1 \psi_L^2 | \frac{e^2}{|\vec{r^1} - \vec{r^2}|} | \psi_L^1 \psi_R^2 \rangle = \langle \psi_R^1 \psi_R^2 | \frac{e^2}{|\vec{r^1} - \vec{r^2}|} | \psi_L^1 \psi_R^2 \rangle, \tag{6c}$$

$$J = \langle \psi_L^1 \psi_R^2 | \frac{e^2}{|\vec{r^1} - \vec{r^2}|} | \psi_R^1 \psi_L^2 \rangle. \tag{6d}$$

The two expressions for U and D are taken to be equal for simplicity.

Obviously, all off-diagonal elements need to be zero in the triplet block, because the spin wave functions are orthogonal and there is no contribution from electron transfer. The energies for the three triplet states are therefore degenerate:

$$E_T = \varepsilon_L + \varepsilon_R + C - J. \tag{7}$$

Diagonalization of the singlet matrix is straightforward but the resulting expressions are somewhat complicated and are therefore deferred to Ref. [15]. Relatively simple results are obtained for the case $\Delta = 0$; setting $\varepsilon_0 = \varepsilon_L = \varepsilon_R$,

$$E_{S,1} = 2\varepsilon_0 + \frac{U + C + 2J}{2} - \sqrt{\frac{(U - C)^2}{4} + 4(t_{\mathrm{MO}} - D)^2}, \tag{8a}$$

$$E_{S,2} = 2\varepsilon_0 + U - J, \tag{8b}$$

$$E_{S,3} = 2\varepsilon_0 + \frac{U + C + 2J}{2} + \sqrt{\frac{(U - C)^2}{4} + 4(t_{\mathrm{MO}} - D)^2}. \tag{8c}$$

Because the on-site interaction term, U, can be assumed to be quite large compared to all other terms, $E_{S,1}$ is usually the lowest singlet level. The spatial parts of the singlet wave functions are written as

$$|S^{(\upsilon)}\rangle = a_{LL}^{(\upsilon)}|S_{LL}\rangle + a_{RR}^{(\upsilon)}|S_{RR}\rangle + a_{LR}^{(\upsilon)}|S_{LR}\rangle. \tag{9}$$

Here the superscripts in parentheses label the three singlet states, i.e., $\upsilon = 1,2,3$ with $\upsilon = 1$ labeling the lowest-energy state.

In nearly all cases the lowest-energy singlet level lies beneath the triplet level. This is particularly the case when Δ is nonzero, as will be discussed further in the following section.

Now we consider the left and right metals. They are modeled by the Hamiltonian:

$$H_{\mathrm{ME}} = -\sum_{n=1}^{N} t_{\mathrm{ME}}(c_n^+ c_{n+1} + \mathrm{H.c.}) - \sum_{n=-1}^{-N} t_{\mathrm{ME}}(c_n^+ c_{n-1} + \mathrm{H.c.}) \tag{10}$$

where $-t_{\mathrm{ME}}$ is the transfer-matrix element in the metal, n labels the sites of the chain in the contact, and N is a large positive integer, as sketched in Fig. 2. A single-electron state characterized by wave number k may be written as $|\psi_k\rangle = \sum_1^N a_n|\psi_n\rangle$ or $\sum_{-1}^{-N} a_n|\psi_n\rangle$. It is readily found that the coefficients for the sites immediately adjacent to the molecule, a_{+1} and a_{-1}, are both given by $(1 - r)/\sqrt{2N}$. Here $r = e^{-2ika}$, a is the lattice constant, k is related to the electron energy by $\varepsilon_k = -2t_{\mathrm{ME}}\cos(ka)$, and the total number of sites, N, provides the proper normalization.

The metal contacts are coupled to the organic molecule through a tunneling Hamiltonian of the form

$$H_T = -\tau_L(c_L^+ c_{-1} + \text{H.c.}) - \tau_R(c_R^+ c_1 + \text{H.c.}) \tag{11}$$

where $-\tau_L$ ($-\tau_R$) is the transfer-matrix element between the metal site immediately adjacent to the molecule on the left (right) side (Fig. 2).

We describe the tunneling process in second-order perturbation theory. Since the virtual intermediate state $|m\rangle$ is a two-electron singlet or triplet state, we also need to consider singlet and triplet states formed by the electron in the molecule interface state [defined by Eq. (3)] and the electron in the emitting or collecting contact as initial, $|i\rangle$, and final, $|f\rangle$, states:

There is one possible initial/final singlet state:

$$|k,S\rangle = \frac{1}{\sqrt{2}}\left(|\psi_k^1\rangle|\psi_{M-}^2\rangle + |\psi_{M-}^1\rangle|\psi_k^2\rangle\right)\frac{1}{\sqrt{2}}(|\uparrow^1\rangle|\downarrow^2\rangle - |\downarrow^1\rangle|\uparrow^2\rangle) \tag{12a}$$

and three possible initial/final triplet states:

$$\left.\begin{matrix}|k,T_+\rangle \\ |k,T_-\rangle \\ |k,T_0\rangle\end{matrix}\right\} = \frac{1}{\sqrt{2}}\left(|\psi_k^1\rangle|\psi_{M-}^2\rangle - |\psi_{M-}^1\rangle|\psi_k^2\rangle\right)\begin{cases}|\uparrow^1\rangle|\uparrow^2\rangle \\ |\downarrow^1\rangle|\downarrow^2\rangle \\ \frac{1}{\sqrt{2}}(|\uparrow^1\rangle|\downarrow^2\rangle + |\downarrow^1\rangle|\uparrow^2\rangle)\end{cases}. \tag{12b}$$

With these wave functions, the following transmission matrix elements are obtained in second-order perturbation theory for singlet and triplet pairing, denoted by S and T subscripts, respectively. For the singlet case, we consider only the lowest-energy singlet state, which yields the lowest tunneling barrier. Following Eq. (9), that state is identified by a superscript (1):

$$|\langle M_S\rangle|^2 = \left|\frac{\langle i|H_T|m\rangle\langle m|H_T|f\rangle}{E_i - E_m}\right|^2 = \frac{|(1-r)|^4\tau_L^2\tau_R^2\left(\sqrt{2}a_{LL}^{(1)}a_{L-} + a_{LR}^{(1)}a_{R-}\right)^2\left(\sqrt{2}a_{RR}^{(1)}a_{R-} + a_{LR}^{(1)}a_{L-}\right)^2}{4N^2(\varepsilon_k + \varepsilon_{\text{MO},-} - E_{S,1})^2}, \tag{13a}$$

$$|\langle M_T\rangle|^2 = \left|\frac{\langle i|H_T|m\rangle\langle m|H_T|f\rangle}{E_i - E_m}\right|^2 = \frac{|(1-r)|^4\tau_L^2\tau_R^2 a_{L-}^2 a_{R-}^2}{4N^2(\varepsilon_k + \varepsilon_{\text{MO},-} - E_T)^2}. \tag{13b}$$

E_i represents the two-particle energy in the initial state, which is $\varepsilon_k + \varepsilon_{\text{MO},-}$, if the Coulomb interaction between an electron in the metal emitter contact and the electron in the molecular interface state is negligible. For small applied bias tunneling is dominated by electrons at the contact Fermi level; hence, $\varepsilon_k = \varepsilon_F$. E_m corresponds to the intermediate state: $E_m = E_{S,1}$ for singlet pairing and $E_m = E_T$ for triplets. The effective tunnel barriers are $E_{S,1} - \varepsilon_{\text{MO},-} - \varepsilon_F$ and $E_T - \varepsilon_{\text{MO},-} - \varepsilon_F$ for singlet and triplet paired electrons at the Fermi level, respectively.

The density of states in the contacts is given by $g(\varepsilon) = 2N/\pi\sqrt{4t_{\text{ME}}^2 - \varepsilon^2}$, which includes the spin degeneracy. We attribute a quarter of the density of states to the singlet and each of the triplet initial and final states.

The transmission rates per unit energy for electrons at energy ε forming singlet and triplet states can therefore be expressed as

$$W_S = \frac{2\pi}{\hbar}\left(\frac{g(\varepsilon)}{4}\right)^2|\langle M_S\rangle|^2 = \frac{\left(4t_{\text{ME}}^2 - \varepsilon^2\right)\tau_L^2\tau_R^2\left(\sqrt{2}a_{LL}^{(1)}a_{L-} + a_{LR}^{(1)}a_{R-}\right)^2\left(\sqrt{2}a_{RR}^{(1)}a_{R-} + a_{LR}^{(1)}a_{L-}\right)^2}{8\pi\hbar(\varepsilon + \varepsilon_{\text{MO},-} - E_{S,1})^2 t_{\text{ME}}^4}, \tag{14a}$$

$$W_T = \frac{2\pi}{\hbar}\left(\frac{g(\varepsilon)}{4}\right)^2|\langle M_T\rangle|^2 = \frac{\left(4t_{\text{ME}}^2 - \varepsilon^2\right)\tau_L^2\tau_R^2 a_{L-}^2 a_{R-}^2}{8\pi\hbar(\varepsilon + \varepsilon_{\text{MO},-} - E_T)^2 t_{\text{ME}}^4}. \tag{14b}$$

B. Spin relaxation

The model constructed in the preceding section essentially defines four parallel transmission channels for the four possible spin configurations in the initial state. Spin relaxation can enable transitions between the transmission channels. This is unlikely to occur in the intermediate (virtual) state, i.e., during the tunneling process, because the energy difference between the singlet and triplet states is significant. However, for the initial states one electron populates the metal emitter contact and its Coulomb interaction with the unpaired electron in the molecular interface state is very weak. Therefore singlet and triplet initial states are nearly degenerate and even relatively weak mechanisms can produce transitions between them. In the real physical system, there are of course a large number of initial singlet and triplet states with different spatial wave functions. In our model, this is reduced to the four states of Eq. (12). Finally, an applied magnetic field splits the energy levels of the triplet states and therefore exercises influence on the transitions between the transmission channels. It is important to stress, however, that the magnetic field induced splitting is very small, such that the thermodynamic effects are entirely negligible [16]. In this section we construct a model for the electron ensemble in the initial state.

The system Hamiltonian, H, includes the Zeeman interaction, H_Z, which is time independent, and a random interaction coupling to the electron spin that fluctuates either in time or space, H_R. This interaction models the effects of scattering, which together with spin-orbit coupling can cause spin flips. It also models the effects of the hyperfine interaction on either electron comprising the pair, which also gives rise to spin relaxation. Lastly, we allow for a small exchange splitting between the singlet and triplet initial states that arises if the

exchange interaction between electrons in the contact and electrons in the interface states of the molecules is not entirely negligible. This effect on the initial states is modeled by the Hamiltonian $H_{\rm ex}$. The energy-level diagram envisioned for the initial state as a function of the applied magnetic field is shown in Fig. 3.

For a particular molecule the two electrons of the initial state are again labeled by superscripts. The Zeeman interaction is written as

$$H_Z = g_1\mu_B s_Z^1 B_Z + g_2\mu_B s_Z^2 B_Z \tag{15}$$

where B_Z is the applied magnetic field, μ_B is the Bohr magneton, and $g_{1,2}$ are the g factors. Using $\bar{g} = (g_1 + g_2)/2$ and $\Delta g = (g_1 - g_2)/2$ we write the interaction as follows:

$$H_Z = \bar{H} + \Delta H = \mu_B\left(s_Z^1 + s_Z^2\right)\bar{g}B_Z + \mu_B\left(s_Z^1 - s_Z^2\right)\Delta g B_Z. \tag{16}$$

The Hamiltonian for the interaction H_R coupling to the electron spins can be written as

$$H_R = \mu_B \vec{B_R^1}\cdot\vec{s^1} + \mu_B \vec{B_R^2}\cdot\vec{s^2}. \tag{17}$$

We first choose $\bar{H}$ as the zeroth-order Hamiltonian, H_0, and $H_P = H_R$ as a perturbation. Subsequently, we will include $H_{\rm ex}$ and ΔH into H_0.

A spin-density matrix is used to describe the ensemble of nonequilibrium electron pairs. The four-dimensional spin Hilbert space is spanned by the singlet and triplet (initial) states. H_0 is diagonalized, and the energies are sketched in Fig. 3. The time evolution of the density matrix, ρ, is given by a stochastic Liouville equation [17]:

$$\frac{d\rho}{dt} = \frac{i}{\hbar}[\rho, H_0 + H_P] + \left.\frac{\partial\rho}{\partial t}\right|_{\rm cre} + \left.\frac{\partial\rho}{\partial t}\right|_{\rm ann}. \tag{18}$$

Here the last two terms describe the creation of initial-state electron pairs by the supply of electrons from the emitting contact and the annihilation of such pairs by the tunneling process, respectively. (To avoid the introduction of additional parameters, contributions to the annihilation term associated with transport away from the metal-molecule interface are suppressed.)

Transforming to an interaction picture representation, we define $\rho^*(t) = e^{(i/\hbar)H_0 t}\rho(t)e^{-(i/\hbar)H_0 t}$, $H_P^* = e^{(i/\hbar)H_0 t} H_P e^{-(i/\hbar)H_0 t}$, and $\rho_0 = \rho(0)$. In second-order iteration, the first term on the right-hand side of Eq. (18) becomes [18]

$$\frac{i}{\hbar}[\rho^*, H_P^*] = \frac{i}{\hbar}[\rho_0^*, H_P^*] + \left(\frac{i}{\hbar}\right)^2 \int_0^t [[\rho_0^*, H_P^*(t')], H_P^*(t)]dt'. \tag{19}$$

Noting that fluctuations in and out of the ensemble of electron pairs through the last two terms in Eq. (18) randomize the phase of the ensemble averaged density matrix, we can take ρ_0^* to be diagonal. Furthermore, using $|j\rangle$ and $|k\rangle$ to label the eigenstates of H_0 we find for the first term on the right-hand side of Eq. (19)

$$[\rho_0^*, H_P^*]_{jk} = \langle j|H_P^*|k\rangle(\rho_{0j}^* - \rho_{0k}^*) \tag{20}$$

and the diagonal elements vanish.

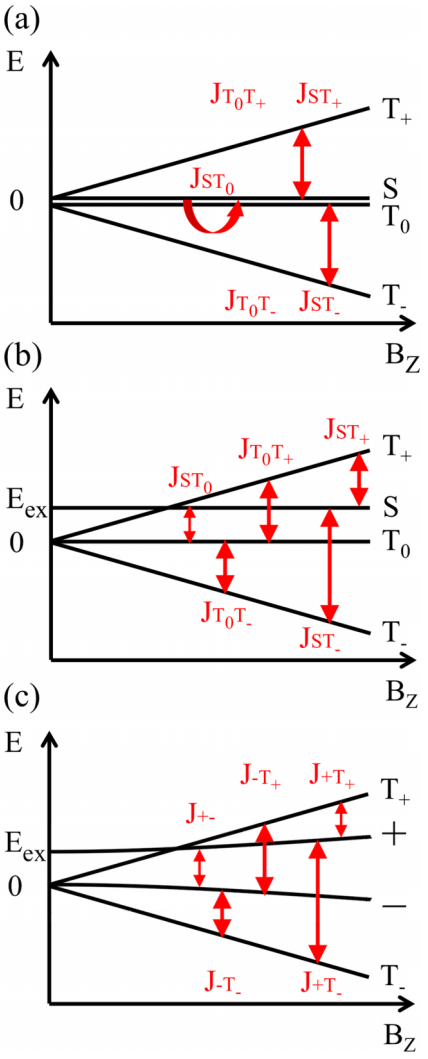

FIG. 3. Schematic energy-level diagrams for the initial singlet and triplet two-electron pair states as a function of the applied magnetic field. (a) Neglecting the small exchange splitting, all levels are degenerate at $B_Z = 0$. (b) Showing the effect of a small exchange splitting, $E_{\rm ex}$. (c) Including the effect of different g factors for the two electrons. Also indicated are the allowed spin-relaxation transitions.

H_P, is taken to vary randomly for the ensemble, and we therefore focus on the ensemble averaged diagonal density-matrix elements, e.g., $\langle j|\rho^*|j\rangle = \langle j|\rho|j\rangle$ [18]. The second term in Eq. (19) yields

$$\frac{-1}{\hbar^2}\int_{-t}^{t}\langle j|\rho_0|j\rangle\sum_k G_{jk}(\tau)e^{i(E_j-E_k)\tau/\hbar}d\tau + \frac{1}{\hbar^2}\int_{-t}^{t}\sum_k\langle k|\rho_0|k\rangle G_{kj}(\tau)e^{-i(E_j-E_k)\tau/\hbar}d\tau. \tag{21}$$

Here, the energy of state $|j\rangle$ is expressed as E_j and the time correlation function, $G_{jk}(\tau) = \overline{\langle j|H_P(t)|k\rangle\langle k|H_P(t+\tau)|j\rangle}$, depends only on the time difference, τ.

The matrix elements of H_P are nonzero only for $\Delta S_Z = 0, \pm 1$. In addition, all $G_{jk}(\tau)$ originate from H_R and are proportional to $\overline{(B_R)^2} = [\overline{(B_R^1)^2} + \overline{(B_R^2)^2}]/12$. Finally, the correlation functions are symmetric around $\tau = 0$ and decrease rapidly

to zero as $|\tau|$ increases because the electrons in the emitting metal contact are mobile and nuclear spins may fluctuate randomly. Using τ_0 to describe a relevant time scale for dephasing of the electron spins, we consider the following simple form:

$$G_{\Delta S_Z=0,\pm1}(\tau) = e^{-|\tau|/\tau_0}\mu_B^2\overline{B_R^2}. \tag{22}$$

Equation (22) clearly constitutes only a simple approximation to a complex problem of perhaps multiple interactions that can contribute to spin relaxation. Other forms of the correlation function have been considered [19–21].

The Fourier transform of the correlation function, given by $J_{jk}(\omega) = \int_{-\infty}^{\infty} G_{jk}(\tau)e^{\frac{i\omega\tau}{\hbar}}/\hbar^2 d\tau \propto \tau/[1+(\omega\tau)^2]$ for $\omega = (E_k - E_j)/\hbar$, then yields the transition rate between states $|j\rangle$ and $|k\rangle$. The effect of the applied magnetic field enters through the Zeeman energy difference, expressed through $\overline{B_Z} = \bar{g}B_Z$. Taking H_0 to be either $\bar{H}$ or $\bar{H} + H_{\rm ex}$, the relevant eigenstates are those of Eq. (12): $|k,S\rangle$, $|k,T_0\rangle$, $|k,T_+\rangle$, and $|k,T_-\rangle$. The transition rates are written as

$$J_{S,T_0} = J_0\frac{1}{1+\left(\frac{B_{\rm ex}}{B_C}\right)^2}, \tag{23a}$$

$$J_{S,T_\pm} = J_0\frac{1}{1+\left(\frac{B_Z\mp B_{ex}}{B_C}\right)^2}, \tag{23b}$$

$$J_{T_0,T_\pm} = J_0\frac{1}{1+\left(\frac{B_Z}{B_C}\right)^2}. \tag{23c}$$

Here $J_0 = 2\tau_0\mu_B^2\overline{B_R^2}/\hbar^2$, $B_C = \hbar/\tau_0\bar{g}\mu_B$, and $B_{\rm ex} = E_{\rm ex}/\bar{g}\mu_B$, as it is convenient to express these energies in magnetic field units.

In Eq. (18), $\partial\rho/\partial t|_{\rm cre}$ is the formation rate of electron pairs in the initial state of the tunneling process. The pair annihilation rare, $\partial\rho/\partial t|_{\rm ann}$, corresponds to the tunneling process and it is expressed in terms of kinetic coefficients K_S and K_T for the singlet and the triplet states, respectively, and the probabilities of the corresponding initial states being occupied as given by the diagonal elements of the density matrix. K_S and K_T are proportional to $W_S(\varepsilon_F)$ and $W_T(\varepsilon_F)$, respectively. The time evolution of the diagonal elements of the density matrix then takes on the form of a master equation:

$$\frac{d\langle j|\rho|j\rangle}{dt} = \left.\frac{\partial\langle j|\rho|j\rangle}{\partial t}\right|_{\rm cre} - K_j\langle j|\rho|j\rangle - \langle j|\rho|j\rangle\sum_k J_{jk} + \sum_k\langle k|\rho|k\rangle J_{kj}. \tag{24}$$

In the following, we define $\delta n_S = \delta n\langle S|\rho_0|S\rangle$, $\delta n_{T_0} = \delta n\langle T_0|\rho_0|T_0\rangle$, $\delta n_{T+} = \delta n\langle T_+|\rho_0|T_+\rangle$, and $\delta n_{T-} = \delta n\langle T_-|\rho_0|T_-\rangle$. Evidently, by normalization of the density matrix, $\delta n = \delta n_S + \delta n_{T_0} + \delta n_{T+} + \delta n_{T-}$. For a nonmagnetic contact, electrons arrive at the metal-molecule interface without spin polarization. Consequently, all four pair states are populated with equal rates. With the pair creation rate denoted by F, one obtains explicitly for the steady state:

$$0 = F - K_S\delta n_S - J_{ST_0}\delta n_S - J_{ST_+}\delta n_S - J_{ST_-}\delta n_S + J_{ST_0}\delta n_{T_0} + J_{ST_+}\delta n_{T_+} + J_{ST_-}\delta n_{T_-}, \tag{25a}$$

$$0 = F - K_T\delta n_{T_0} - J_{ST_0}\delta n_{T_0} - J_{T_0T_+}\delta n_{T_0} - J_{T_0T_-}\delta n_{T_0} + J_{ST_0}\delta n_S + J_{T_0T_+}\delta n_{T_+} + J_{T_0T_-}\delta n_{T_-}, \tag{25b}$$

$$0 = F - K_T\delta n_{T_+} - J_{ST_+}\delta n_{T_+} - J_{T_0T_+}\delta n_{T_+} + J_{ST_+}\delta n_S + J_{T_0T_+}\delta n_{T_0}, \tag{25c}$$

$$0 = F - K_T\delta n_{T_-} - J_{ST_-}\delta n_{T_-} - J_{T_0T_-}\delta n_{T_-} + J_{ST_-}\delta n_S + J_{T_0T_-}\delta n_{T_0}. \tag{25d}$$

The tunneling current is simply given by $I = eK_S\delta n_S + eK_T(\delta n_{T_0} + \delta n_{T+} + \delta n_{T-}) = 4F$. The voltage drop across the molecules, on the other hand, is proportional to the number of accumulated electrons, i.e., proportional to δn, and it depends on the applied magnetic field B_Z. Consequently the resistance, which is proportional to $\delta n/I$, also depends on the magnetic field, but it is independent of F. The relative magnetoresistance may be defined as

$$\mathrm{MR}(B_Z) = \left[(\delta n/I)_{B_Z} - (\delta n/I)_{B_Z=0}\right]/(\delta n/I)_{B_Z=0}. \tag{26}$$

Adding the term ΔH defined in Eq. (16) to H_0 introduces mixing of the states $|k,S\rangle$ and $|k,T_0\rangle$ and modifies the energy levels as shown schematically in Fig. 3(c). The eigenfunctions of this modified H_0 are labeled $|k,+\rangle$, $|k,-\rangle$, $|k,T_+\rangle$, and $|k,T_-\rangle$. The last two are unaffected by ΔH, as are their energy levels. The first two are given by

$$|k,+\rangle = A_S^+|k,S\rangle + A_{T_0}^+|k,T_0\rangle, \tag{27a}$$

$$|k,-\rangle = A_S^-|k,S\rangle + A_{T_0}^-|k,T_0\rangle, \tag{27b}$$

$$A_S^\pm = \frac{\bar{g}B_\pm/\Delta g B_Z}{\sqrt{1+(\bar{g}B_\pm/\Delta g B_Z)^2}}, \tag{28a}$$

$$A_{T_0}^\pm = \frac{1}{\sqrt{1+(\bar{g}B_\pm/\Delta g B_Z)^2}}. \tag{28b}$$

Here, $B_\pm = E_\pm/\bar{g}\mu_B$ and the energy levels are given by

$$E_\pm = \frac{\bar{g}\mu_B B_{\rm ex}}{2} \pm \sqrt{\frac{(\bar{g}\mu_B B_{\rm ex})^2}{4} + (\Delta g\mu_B B_Z)^2}. \tag{29}$$

The transition rates are affected by these modifications and acquire the following forms:

$$J_{+,-} = J_0\left(A_S^+A_{T_0}^- + A_S^-A_{T_0}^+\right)^2\frac{1}{1+\left(\frac{B_+-B_-}{B_C}\right)^2}, \tag{30a}$$

$$J_{+,T_\pm} = J_0\frac{1}{1+\left(\frac{B_+\mp B_Z}{B_C}\right)^2}, \tag{30b}$$

$$J_{-,T_\pm} = J_0\frac{1}{1+\left(\frac{B_-\mp B_Z}{B_C}\right)^2}. \tag{30c}$$

III. RESULTS AND DISCUSSION

To estimate the MR expected from the model constructed, a discussion of suitable parameters is required. Beginning with the Coulomb terms we note that if the local spatial wave functions are taken to be s orbitals, $\psi_L(\vec{r}) \propto \exp(-\beta|\vec{r} + \hat{u}_x d/2|)$ and $\psi_R(\vec{r}) \propto \exp(-\beta|\vec{r} - \hat{u}_x d/2|)$, where d is the distance between the two sites in the molecule ($1/\beta < d$), all Coulomb terms are positive. Furthermore, we may use $C_0 = e^2/d$ as the scale parameter and write $U \approx \gamma C_0$, $C \approx C_0$, $D \approx \alpha C_0$, and $J \approx \alpha^2 C_0$, where $\alpha \approx e^{-\beta d} < 1$ and $\gamma > 1$. Under these conditions E_{S1} is significantly less than E_{S2} and E_{S3}, hence

TABLE I. Example parameters for the intramolecular Coulomb interaction, the transfer-matrix element within the molecule, the transfer-matrix element within the metal contacts, and the transfer-matrix elements between the contacts and the molecule. The upper line shows the Coulomb energies normalized by the intramolecular or transfer-matrix element and the molecule-metal coupling matrix element normalized by the metal transfer-matrix element.

	U	C	D	J	t_{MO}	t_{ME}	τ_L	τ_R	
E/t_{MO}	5	1	0.2	0.04	1	1	0.05	0.05	E/t_{ME}
E (eV)	5	1	0.2	0.04	1	2	0.1	0.1	E (eV)

the E_{S1} level dominates the singlet tunneling process. Furthermore, $E_{S1} < E_T$ unless $2(U-C)J + 4J^2 > 4(t_{\mathrm{MO}} - D)^2$. Allowing for nonzero Δ makes it more difficult to achieve a situation in which the triplet energy level is below the lowest singlet level. Example parameters are listed in Tables I and II.

In Fig. 4, the transmission rates W_S and W_T are graphed as functions of the electron energy, ε, varying over the metal bandwidth ($-2t_{\mathrm{ME}} < \varepsilon < 2t_{\mathrm{ME}}$). The mean energy of the left and right site single-electron energy levels in the molecule, $\bar{\varepsilon} = (\varepsilon_L + \varepsilon_R)/2$, is set to zero. The energy splitting caused by the magnetic field is negligibly small compared to the Coulomb interaction. The dashed line represents $\varepsilon_{\mathrm{MO},-}$. ε_F must be greater than $\varepsilon_{\mathrm{MO},-}$, otherwise the interface state is unoccupied and no unpaired electron exists. In addition, ε_F needs to be smaller than the lowest resonance level, usually $E_{S,1} - \varepsilon_{\mathrm{MO},-}$, else that state would be occupied by two electrons and could not facilitate tunneling. (In addition, the transmission resonance exceeds the range of validity of the perturbation theory treatment used.) For the parameters in Table I, a large t_{MO} is used, which leads to a significant splitting between $\varepsilon_{\mathrm{MO},-}$ and $\varepsilon_{\mathrm{MO},+}$. The energy for the singlet state $E_{S,1}$ is always lower than that of the triplet state E_T, Figs. 4(a) and 4(b). However, for small t_{MO} values, as in Table II, $E_{S,1}$ is greater than E_T if Δ is small [Fig. 4(c)]. For large Δ values $E_{S,1}$ is again lower than E_T [Fig. 4(d)]. We also note that for large Δ values [Figs. 4(b) and 4(d)] the singlet linear combination of local orbital states is more favorable for electron transmission than the triplet combination. This provides additional enhancement of W_S relative to W_T in the energy range of interest, $\varepsilon_{\mathrm{MO},-} < \varepsilon < E_{S,1} - \varepsilon_{\mathrm{MO},-}$.

The key result of this model is that, with tunnel barriers on the order of 1 eV, ratios $W_S/W_T = K_S/K_T$ greater than 10 are readily obtained, but ratios less than 1 are also possible for certain parameter values.

To explore the magnetoresistance associated with tunneling of electrons through the molecule, we normalize Eqs. (25a)–(25d) by J_0 and define $k_S = K_S/J_0$, $k_T = K_T/J_0$. The

TABLE II. Alternative set of model parameters with a significantly smaller intramolecular transfer-matrix element. All other parameters are the same as those of Table I.

	U	C	D	J	t_{MO}	t_{ME}	τ_L	τ_R	
E/t_{MO}	50	10	2	0.4	1	1	0.05	0.05	E/t_{ME}
E (eV)	5	1	0.2	0.04	0.1	2	0.1	0.1	E (eV)

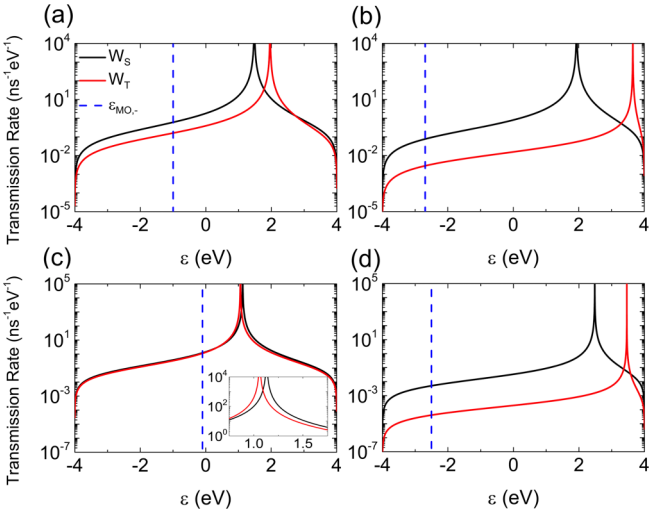

FIG. 4. Transmission rates for singlet (red) and triplet (black) states plotted as functions of ε with (a) $\Delta = 0$, (b) $\Delta = 5t_{\mathrm{MO}} = 5\,\mathrm{eV}$, (c) $\Delta = 0$, and (d) $\Delta = 50t_{\mathrm{MO}} = 5\,\mathrm{eV}$. The parameters for (a) and (b) are in Table I. The parameters for (c) and (d) are in Table II. The dashed lines indicate $\varepsilon_{\mathrm{MO},-}$.

magnetic field scales are given by $(\overline{B_R^2})^{1/2}$ and by B_C. As these quantities are associated with the rather weak interactions that cause spin relaxation, we estimate them to be on the order of 1−100 mT.

Figure 5 shows MR as a function of the ratio of k_S/k_T and the applied magnetic field. In Fig. 5(a) both B_{ex} and Δg are taken to be zero, i.e., $H_0 = \bar{H}$. With B_Z increasing and the ratio of k_S/k_T deviating from 1, transitions $|S\rangle \leftrightarrows |T_\pm\rangle$ and $|T_0\rangle \leftrightarrows |T_\pm\rangle$ are increasingly suppressed, and the overall transmission decreases. Hence, for fixed current, more electrons accumulate at the interface between the emitting contact and the SAM of molecules leading to positive MR.

Considering now a case of nonzero exchange splitting between the initial singlet and triplet states, i.e., $H_0 = \bar{H} + H_{\mathrm{ex}}$, a B_Z value equal to B_{ex} leads to degeneracy of the $|S\rangle$ and $|T_+\rangle$ states, as shown in Fig. 3(b), and therefore enables rapid electron transfer between these states. Consequently, negative MR is achieved in this field range if $k_S/k_T \neq 1$. Finally, positive MR again results for large magnetic fields if $k_S \ll k_T$. This is depicted in Fig. 5(b).

Figure 5(c) shows the effects of a difference in g factors of the two electrons in the initial state. Regarding an estimate for Δg we note that the g factor for gold conduction electrons is about 2.2 [22] while the g factor for organic molecules consisting of only light atoms is usually taken to be equal to 2 [23]. Hence, we use $\Delta g = 0.1$ for the example results. This introduces a new phenomenon. When the applied magnetic field is sufficiently large the coupling between the $|k,S\rangle$ and $|k,T_0\rangle$ states induced by $\Delta H(B_z \gg B_{\mathrm{ex}})$ maximizes the transmission effectiveness of these two channels and therefore reduces the resistance, yielding negative MR.

Finally, the calculated MR(B_Z) is plotted for $\Delta g = 0$ and 0.1 and different B_{ex} values in Figs. 6(a) and 6(b). In general, a magnetic field tends to separate the energy levels of the initial state, therefore inhibiting transitions and leading to positive MR. Furthermore, an energy splitting between $|S\rangle$ and $|T_0\rangle$

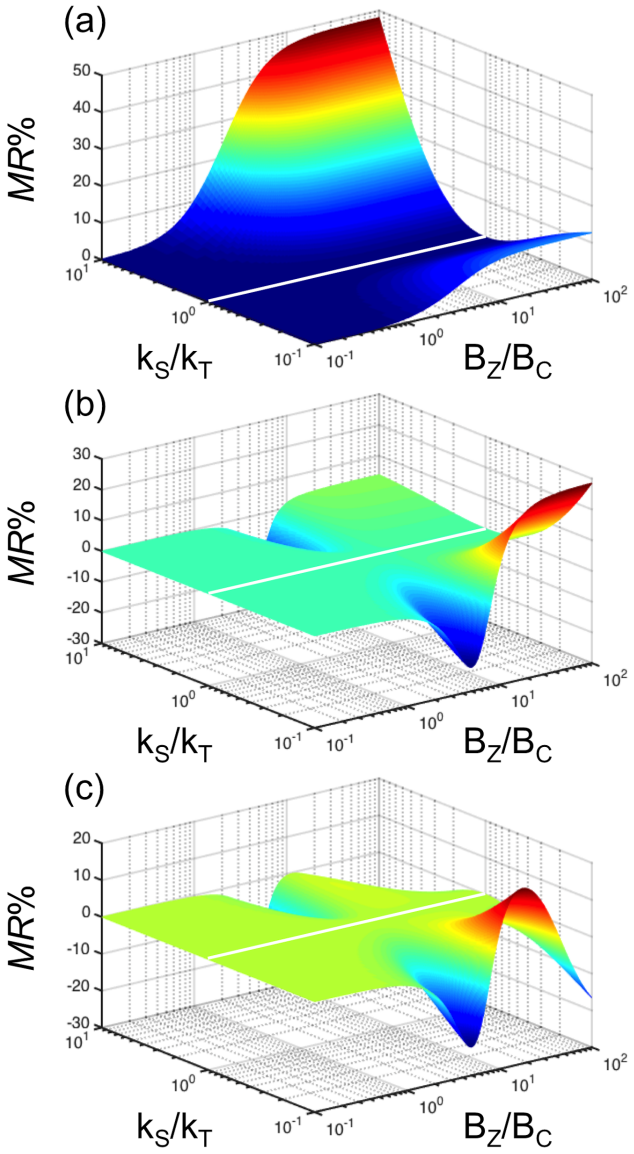

FIG. 5. MR as a function of the applied magnetic field and k_S/k_T, with (a) $B_{\rm ex}/B_C = 0$, $\Delta g = 0$, $k_T = 0.5$; (b) $B_{\rm ex}/B_C = 5$, $\Delta g = 0$, $k_T = 0.5$; and (c) $B_{\rm ex}/B_C = 5$, $\Delta g = 0.1$, $k_T = 0.5$.

states ($B_{\rm ex}$) reduces the transition rates between singlet and all triplet states for $B_Z = 0$. If $B_{\rm ex}$ is large, all transition rates are small compared to the tunneling rates. The transition rate J_{S,T_+}, however, reaches a maximum for $B_Z = B_{\rm ex}$, resulting in a decrease of the resistance, i.e., negative MR, in that field range. This is evident in both Figs. 6(a) and 6(b). Figure 6(b) includes the effects of nonzero Δg on MR. The new feature of negative MR appearing here at low magnetic fields for the case of small $B_{\rm ex}$ is again due to the mixing of the $|k,S\rangle$ and $|k,T_0\rangle$ states induced by $\Delta H(B_z)$, which maximizes the transmission effectiveness of these two channels and therefore reduces the resistance.

Evidently, MR(B_Z) approaches constant values for large magnetic fields. These values depend on k_S, k_T, and $B_{\rm ex}$ and Δg. The general expressions are rather complicated and therefore shown only in Ref. [15]. However, two simple limiting cases are worth presenting here. If $B_{\rm ex}/B_C \gg 1$ and

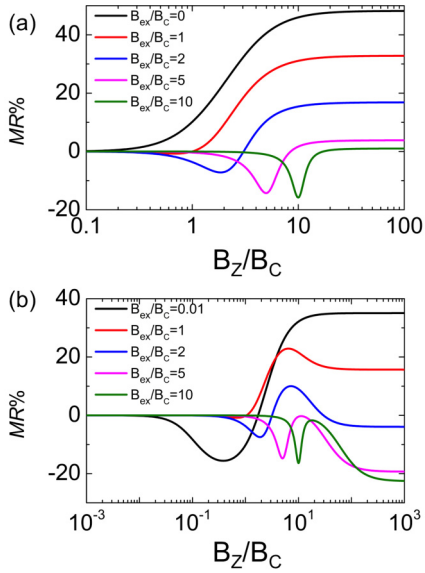

FIG. 6. (a) MR(B_Z) for $B_{\rm ex}/B_C = 0, 1, 2, 5, 10$. $\Delta g = 0$, $k_S = 5$, and $k_T = 0.5$. (b) MR(B_Z) for $B_{\rm ex}/B_C = 0.01, 1, 2, 5, 10$. $\Delta g = 0.1$, $k_S = 5$, and $k_T = 0.5$.

$\Delta g = 0$, one readily finds that MR $= 0$ for $B_Z/B_C \gg 1$. On the other hand, $B_{\rm ex}/B_C \gg 1$ and $\Delta g \neq 0$ yields MR $= -(k_t - k_s)^2/(k_t + k_s)(k_t + 3k_s)$ for $B_Z/B_C \gg 1$. These results are also seen in Figs. 6(a) and 6(b). It should be noted, however, that the limit $B_{\rm ex}/B_C \gg 1$ is meaningful only if B_C is small so the exchange splitting of the initial states is still negligible on the scale of the thermal energy and the existence of equal creation rates for singlet and triplet initial pairs is still a valid assumption.

IV. SUMMARY AND CONCLUSIONS

We have presented an analytical model for charge-carrier transmission through organic molecular tunnel junctions with nonmagnetic electrodes. The Coulomb interaction between the tunneling electron and an unpaired electron populating an interface state leads to significant differences in the transmission barriers for singlet and triplet states. Consequently, the transmission probability of an electron in the emitter contact depends on its spin, i.e., on its population of a singlet or triplet initial state with the unpaired interface state electron. These different pairings constitute separate transmission channels. For a wide range of plausible parameters we find that the transmission probability of the singlet channel exceeds that of the triplet channel.

Spin relaxation through relatively weak interactions of the electrons with their environment can enable transitions between the singlet and triplet transmission channels in the initial state for which the electron-electron interaction is weak and singlet and triplet energies are nearly equal. A small applied magnetic field can lift this degeneracy through the Zeeman interaction and therefore suppress the transitions between singlet/triplet channels, giving rise to strong magnetoresistance. In the simplest cases the magnetoresistance is positive. This agrees with the experimental data reported in Ref. [10], and we consider it to be the baseline result of our model. However, we also find that a small exchange splitting of

the initial-state energy levels and a difference in the g factors of the electrons forming the initial state pairs can result in negative magnetoresistance over certain field ranges.

In the model examples discussed here we considered only relatively simple cases. Specifically, both contacts were modeled identically and the transfer-matrix elements between the molecule and the emitting and collecting contacts were taken to be the same. Real systems explored experimentally may differ. For example, in Ref. [10] several different oligophenylene thiol molecules were investigated. The molecules formed SAMs on gold and were in turn contacted by a gold atomic force microscopy probe. Zero-bias magnetoresistance on the order of 30% was observed for magnetic fields of only 0.1 T at room temperature. It was furthermore found that oligophenylenes of different length yielded the exponential length dependence expected for nonresonant tunneling, but the relative magnetoresistance was approximately the same. The results of the model discussed here are consistent with this finding, allowing for the generalization that one of the transfer-matrix elements, e.g., τ_R, includes the tunneling process through most of the molecule, with the exception of the thiolated end. τ_R then depends exponentially on the length of the molecule and can cancel out in the result for the relative magnetoresistance, as was discussed in Ref. [10].

ACKNOWLEDGMENTS

S.S. gratefully acknowledges a University of Minnesota Graduate School Doctoral Dissertation Fellowship. Access to the facilities of the Minnesota Supercomputing Institute is gratefully acknowledged. This work was supported in part by NSF (Grant No. ECCS-1407473).

[1] F. Chen, X. Li, J. Hihath, Z. Huang, and N. Tao, Effect of anchoring groups on single-molecule conductance: Comparative study of Thiol-, Amine-, and carboxylic-acid-terminated molecules, J. Am. Chem. Soc. **128**, 15874 (2006).

[2] S. Datta, W. Tian, S. Hong, R. Reifenberger, J. I. Henderson, and C. P. Kubiak, Current-Voltage Characteristics of Self-Assembled Monolayers by Scanning Tunneling Microscopy, Phys. Rev. Lett. **79**, 2530 (1997).

[3] C. A. Nijhuis, W. F. Reus, and G. M. Whitesides, Molecular rectification in metal-sam-metal oxide-metal junctions, J. Am. Chem. Soc. **131**, 17814 (2009).

[4] V. B. Engelkes, J. M. Beebe, and C. D. Frisbie, Length-dependent transport in molecular junctions based on SAMs of alkanethiols and alkanedithiols: Effect of metal work function and applied bias on tunneling efficiency and contact resistance, J. Am. Chem. Soc. **126**, 14287 (2004).

[5] S. H. Choi, B. Kim, and C. D. Frisbie, Electrical resistance of long conjugated molecular wires, Science **320**, 1482 (2008).

[6] C. Joachim, J. K. Gimzewski, R. R. Schlittler, and C. Chavy, Electronic Transparence of a Single C_{60} Molecule, Phys. Rev. Lett. **74**, 2102 (1995).

[7] L. Limot, J. Kröger, R. Berndt, A. Garcia-Lekue, and W. A. Hofer, Atom Transfer and Single-Adatom Contacts, Phys. Rev. Lett. **94**, 126102 (2005).

[8] R. Temirov, A. Lassise, F. B. Anders, and F. S. Tautz, Kondo effect by controlled cleavage of a single-molecule contact, Nanotechnology **19**, 065401 (2008).

[9] R. Frisenda, R. Gaudenzi, C. Franco, M. Mas-Torrent, C. Rovira, J. Veciana, I. Alcon, S. T. Bromley, E. Burzurí, and H. S. J. van der Zant, Kondo effect in a neutral and stable all organic radical single molecule break junction, Nano Lett. **15**, 3109 (2015).

[10] Z. Xie, S. Shi, F. Liu, D. L. Smith, P. P. Ruden, and C. D. Frisbie, Large magnetoresistance at room temperature in organic molecular tunnel junctions with nonmagnetic electrodes, ACS Nano **10**, 8571 (2016).

[11] G. Heimel, L. Romaner, J.-L. Brédas, and E. Zojer, Interface Energetics and Level Alignment at Covalent Metal-Molecule Junctions: π-Conjugated Thiols on Gold, Phys. Rev. Lett. **96**, 196806 (2006).

[12] G. Heimel, L. Romaner, E. Zojer, and J.-L. Brédas, Toward control of the metal-organic interfacial electronic structure in molecular electronics: A first-principles study on self-assembled monolayers of π-conjugated molecules on noble metals, Nano Lett. **7**, 932 (2007).

[13] G. Heimel, L. Romaner, E. Zojer, and J.-L Brédas, The interface energetics of self-assembled monolayers on metals, Acc. Chem. Res. **41**, 721 (2008).

[14] I. Bâldea and H. Köppel, Sources of negative differential resistance in electric nanotransport, Phys. Rev. B **81**, 193401 (2010).

[15] See Supplemental Material at http://link.aps.org/supplemental/10.1103/PhysRevB.95.155315 for a derivation of the singlet state energies and wavefunctions of Sec. II A of the main text for the general case of arbitrary Δ; the derivation of magnetoresistance for Sec. III of the main text.

[16] F. Wang, F. Macià, M. Wohlgenannt, A. D. Kent, and M. E. Flatté, Magnetic Fringe-Field Control of Electronic Transport in an Organic Film, Phys. Rev. X **2**, 021013 (2012).

[17] R. Kubo, Stochastic liouville equations, J. Math. Phys. **4**, 174 (1963).

[18] C. P. Slichter, *Principles of Magnetic Resonance*, 3rd ed. (Springer, Urbana, 1990).

[19] F. Liu, M. R. Kelley, S. A. Crooker, W. Nie, A. D. Mohite, P. P. Ruden, D. L. Smith, and P. P. Ruden, Magneto-electroluminescence of organic heterostructures: Analytical theory and spectrally resolved measurements, Phys. Rev. B **90**, 235314 (2014).

[20] S. Shi, F. Liu, D. L. Smith, and P. P. Ruden, in *Magneto-Optical Effects in Organic Semiconductor Devices, in Organic Spintronics*, edited by Z.V. Vardeny (World Scientific, Singapore, 2017).

[21] Y. Wang, K. Sahin-Tiras, N. J. Harmon, M. Wohlgenannt, and M. E. Flatté, Immense Magnetic Response of Exciplex Light Emission due to Correlated Spin-Charge Dynamics, Phys. Rev. X **6**, 011011 (2016).

[22] G. E. Grechnev, N. V. Savchenko, I. V. Svechkarev, M. J. G. Lee, and J. M. Perz, Conduction-electron g factors in the noble metals, Phys. Rev. B **39**, 9865 (1989).

[23] H. Haashi, *Introduction to Dynamic Spin Chemistry: Magnetic Field Effects upon Chemical and Biochemical Reactions* (World Scientific, Singapore, 2004).